An Astigmatic Unstable Resonator with an Intracavity Deformable Mirror

D. R. Neal
Sandia National Laboratories; Albuquerque, New Mexico 87185
P. L. McMillin
Kaman Aerospace Corporation; Tucson, Arizona 85711
R. B. Michie
Mission Research Corporation; Albuquerque, New Mexico 87106

SAND--91-2850C

DE91 018815

ABSTRACT

Many side-pumped lasers exhibit significant index gradients across the gain region aperture. For pulsed lasers where these gradients are time dependent, extraction with good beam quality requires the use of an adaptive optic. Since these inhomogeneities are systematic, wavefront correction can be performed with a modal deformable mirror. We have designed a resonator which uses a cylindrically deformable mirror to correct for wavefront aberrations in a pulsed nuclear-reactor-driven laser. The mirror is capable of correcting up to ten waves of cylindrical focus error while maintaining tip/tilt alignment of the resonator. It is based around flat plate bending using magnetostrictive actuators. A cylindrical intracavity beam expander is used to image the DM into the laser gain region. The beam expander can be adjusted to vary the resonator magnification in one axis, or to control the stability of the resonator. The mirror is controlled closed loop using a four channel wavefront sensor and a digital control system.

1. INTRODUCTION

Side-pumped lasers can exhibit significant index of refraction variations across the laser aperture because of nonuniform energy deposition in the gain medium. This greatly complicates design of a laser resonator for energy extraction. For strong pumping, the index variations can be quite large in long-pulse lasers[1,2,3], and vary strongly with time. While it is possible to extract energy with a stable or stable-unstable resonator, the beam quality for a large aperture laser is poor[3]. Thus in order to extract energy efficiently with good beam quality an adaptive optic is necessary. In previous work[3] we developed concepts for stable, stable-unstable and unstable resonators. In this work we develop the unstable resonator concept with an intracavity deformable mirror. While this work is primarily aimed at extracting energy from a nuclear-reactor-pumped laser, it is also applicable to other side pumped lasers such as dye[4] and solid state[5].

A number of issues must be explored in the design of a resonator for such a gain region. Since the index of refraction variations can be large, they must be included in the design of the resonator. The index gradient strength, temporal history and shape must be measured. Wavefront measurements for a nuclear-reactor-driven laser gain region are presented.

Once the index of refraction field is known, a method for correcting the wavefront errors must be developed. For an unstable resonator, we have conceived a deformable mirror inside the laser cavity. Since the aberrations are fairly systematic, a modal deformable mirror[10,11,12] was chosen as simplest to implement. The laser gain region is imaged onto this mirror with an intracavity beam expander that also gives independent magnification control in one direction. The deformable mirror must be capable of correcting for large dynamic wavefront variations in a short time. We have selected a modal deformable mirror driven with magnetostrictive actuators based on the largely parabolic behavior of the index of refraction.

In order to drive the deformable mirror with the proper error signals, a wavefront sensor and control system are an integral part of the resonator design. For a pulsed laser this is difficult since the sensor does not receive sufficient signal at early time. Therefore we used a separate probe laser and dichroic mirrors to sense the laser wavefront error.

The resonator was designed using geometric optics ray tracing to pick curvatures of surfaces and determine the requirements for the deformable mirror. Ray tracing can also be used to determine alignment and design sensitivities. The ray tracing, coupled with physical optics modelling is used to make prediction of resonator performance.

2. LASER GAIN REGION DESCRIPTION

The basic pumping geometry for a slab laser is depicted in Figure 1. The pumping occurs across the x-direction. Lasing is along the z-direction. Since the energy deposition mechanism is range dependent, in the x-direction there is considerable gain and index of refraction

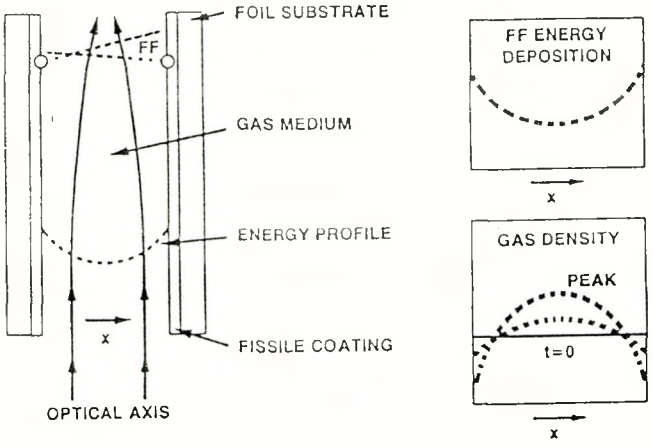

Figure 1: Geometry for wall pumped slab laser. The pumping direction is across the x-direction.

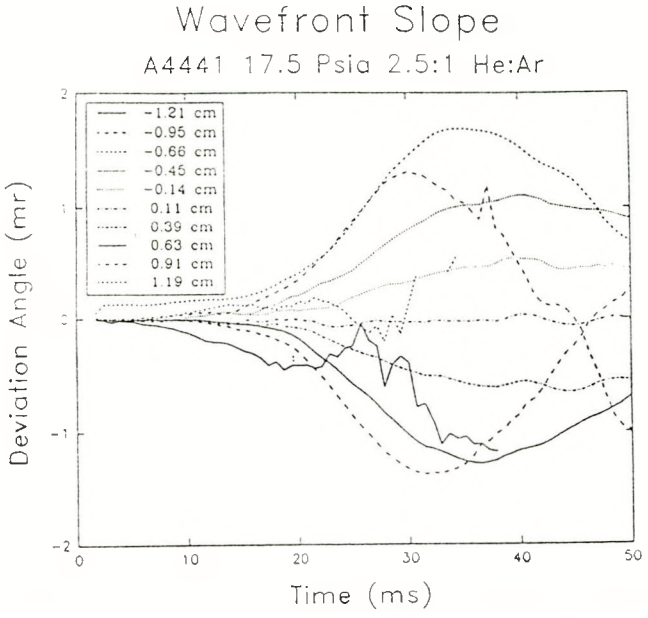

Figure 2: Measured wavefront slopes as a function of time for different positions in the laser aperture. The laser cell was 60 cm long with a 1.5×7 cm aperture. The cell was filled with 15 psi of argon initially at room temperature. The total energy deposited was 410 mJ/cm^3.

variation.

2.1 Index gradient evolution

The index of refraction field for a long-pulse nuclear-reactor-pumped slab laser has been measured in previous work[1,2]. Since the energy deposition in a side-pumped laser is a function of the absorption depth in the laser medium, more energy is deposited near the wall than in the center of the channel. For slab geometries, this will lead to an approximately parabolic index field for most pumping conditions, although higher order terms are important for some conditions[6]. For a pulsed laser the strength of the index gradient will increase monotonically with time during the pumping pulse. The strength of the index gradient is a function of the laser gas composition, pressure, temperature, energy deposition rate, and the absorption depth of the laser medium. For nuclear reactor-pumped lasers this leads to strong index gradients that vary continuously during the 2–10 ms pumping pulse.

Figure 2 is an example of the measured wavefront slope from such a laser. In this case the laser gas was predominately argon at 15 psi. The reactor deposited 410 mJ/cm^3 in a 12 ms FWHM Gaussian pulse. The wavefront slopes varied from an initial zero up to ~1.5 mrad after the peak of the pulse. Thermal relaxation ameliorates the index gradients once the pumping pulse is over, and thus the wavefront slopes slowly decrease with time after about 30 ms. Figure 3 presents a three dimensional depiction of the wavefront error as it evolves with time.

The wavefront profile is nearly parabolic over much of the pumping pulse. This can be seen in Fig. 3, which is the wavefront error derived by integrating the wavefront slopes of Fig. 2. For a long pulse laser, thermal relaxation causes the development of strong higher order terms. For the most part, these terms are important only either very near the wall, or late in the pumping pulse. This data is consistent with previous measurements with shorter pumping pulses[1] and with gas dynamic modelling[8].

For most of the laser aperture, over most of the laser pulse, the index of refraction variations are well approximated by a parabola. Since these variations are quite strong (1–5 mrad) and are relatively rapid (10–20 ms), it is difficult to conceive conventional multi-actuator deformable mirrors that would be capable of achieving both the required dynamic range and bandwidth. We have conceived a special purpose deformable mirror based on modal bending of an initially flat plate. Under appropriate boundary conditions, such a plate will bend into a pure parabolic shape.

If the wavefront error is approximated as a parabola, and since the index variations arise through integration of light rays along the length the gain media, it is appropriate to model the index field as a quadratic duct. Following the development in Siegman[7] and Neal[3]:

$$n(x) = n_0 - \frac{1}{2} n_2{}^* (x/x_{\text{wall}})^2 \qquad (1)$$

where x_{wall} is the half width of the laser cell normal to the

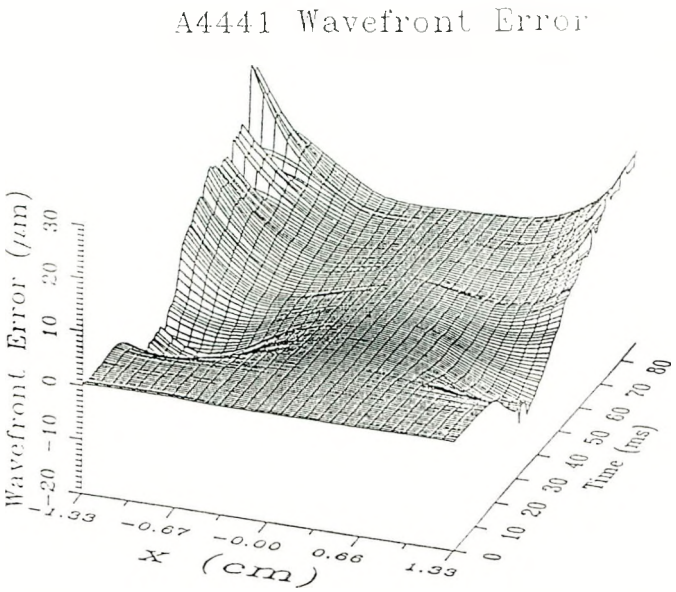

Figure 3: Measured wavefront error as a function of position and time for the 60 cm cell described in Fig. 2. The wavefront error is obtained by integrating the wavefront slopes at each time point. The strong gradients near the wall for late time are due to thermal cooling of the gas by the walls.

pumping direction, $n(x)$ is the index or refraction, and n_0 and $n_2{}^*$ are the appropriate expansion coefficients[3]. Note that Corvo[6] has extended this expansion to higher order.

The *index gradient strength parameter* is defined as:

$$\gamma^* = \sqrt{\frac{n_2{}^*}{n_0}}\frac{L_g}{x_{\text{wall}}} \tag{2}$$

where L_g is the gain region length. This is important since it allows us to represent the index of refraction over the entire aperture with a single quantity. For the slab gain regions discussed in this paper, this represents the index gradient strength in the direction normal to the pumping walls. For slab lasers the pumping nonuniformities in the other directions are generally much smaller, and will be treated as uniform. Thus the index of refraction variations can act a cylindrical lens with a variable focal length.

Using the index gradient strength parameter, the normalized ray matrix can be written:

$$\begin{bmatrix} A & B \\ C & D \end{bmatrix} = \begin{bmatrix} \cos\gamma^* & L_g \sin\gamma^*/n_0\gamma^* \\ -n_0\gamma^* \sin\gamma^*/Lg & \cos\gamma^* \end{bmatrix} \tag{3}$$

This will allow ray tracing through this region in a straightforward fashion.

3. UNSTABLE RESONATOR DESIGN

The resonator design must consider all of the various aspects of the laser and optical system. Correction for the index of refraction variations with the deformable mirror is an integral part of this design. Thus the limits of the deformable mirror are included in this design process. In addition, the control system must be provided with signals describing the output wavefront error of the system. Since this is a pulsed laser, we can not rely on the laser beam itself for wavefront sensing. In a pulsed laser, the initial intensity is zero, giving erroneous information to the control system. Therefore a separate laser is needed that continuously probes the gain medium and deformable mirror. The use of dichroic coatings on resonator optics provides a convenient method for injecting and separating this beam.

Since the laser aperture for efficient pumping with the nuclear reactor driven source is only 1.5 cm, the gradients in the index of refraction are quite large. Constructing a mirror that could produce such large mirror slopes would be very difficult. In specifying the mirror, we assumed that we would be able to expand the laser beam onto the mirror to minimize the required gradients. The wavefront error requirements would remain constant after beam expansion, but the curvature would be greatly reduced.

The need for an intracavity beam expander can be coupled with its use for other functions. The beam expander can be used to image the deformable mirror to the appropriate principle planes of the gain media, and can be used to provide the proper round trip magnification. Furthermore, if the beam expander is cylindrical, it can be used to provide independent control of the magnification in the x and y directions.

In previous work[3] a stable-unstable resonator was used to overcome stability problems associated with the changing index field. The stable-unstable resonator was designed so that the resonator would remain stable in one direction over the range of the strongest expected gain medium focussing. In the orthogonal direction, where the index field was essentially unperturbed, an unstable resonator was used. Energy extraction was accomplished entirely in the unstable direction. Since the aspect ratio of the gain region is large (7:1.5), we have adopted the concept of extraction in a single direction. This is possible since the magnifications are individually adjustable. If the beam expander is remotely adjustable, it is possible to perform both astigmatic (i.e. different M_x and M_y) unstable resonator, and stable-unstable resonator ($M_x < 1$) experiments. This is accomplished by adjusting only the separation of the beam expander elements.

Figure 4 shows the complete system. The primary is a spherical element, selected in conjunction with the cylindrical secondary and the expected cavity length to give

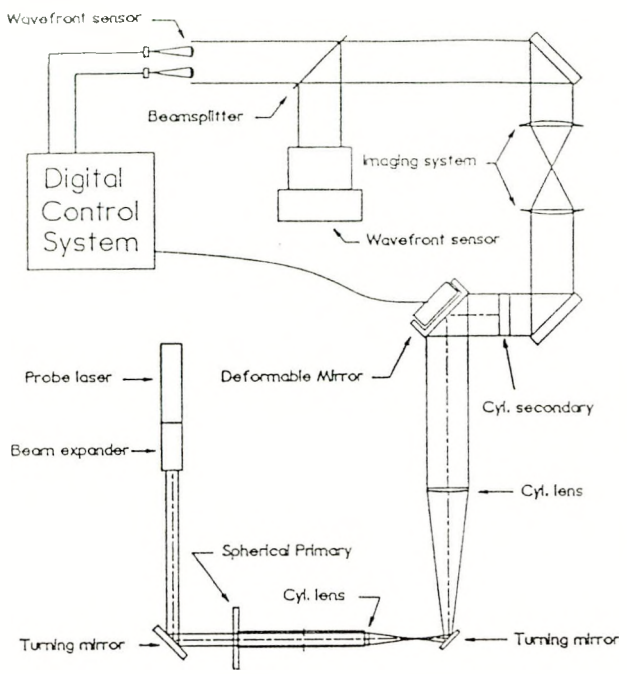

Figure 4: Layout of the Unstable Resonator with Intracavity Deformable Mirror. The primary mirror of the unstable resonator serves as one pressure boundary, and the first element of the beam expander as the other boundary.

a magnification of 2.26. This magnification was chosen to be near optimum output coupling for this gain region based on a Rigrod laser output analysis. Once these mirrors have been selected, the magnification M_y is fixed. The spherical primary mirror is 3 inches in diameter, and is used as a pressure boundary to the cell. It is coated with a dichroic coating with high reflectivity at the lasing wavelengths (1.73 and 2.03 μm), and high transmission at the probe laser wavelength (0.633 μm).

The other pressure boundary is the first element of the cylindrical beam expander. This eliminates the need for windows and their associated losses, but complicates the design of the window/lens holder. The holder has precise tolerances to eliminate the need for adjustment of this optic.

Optical modelling of the laser gain region indicated that the principle planes initially are at the center of the cell. As the pulse progresses and the index gradients increase, the principle planes move apart symmetrically. Since we intend to use a single deformable mirror, we selected the center of the cell as the appropriate location for the image of the mirror. Since the principle planes do not move very much, this was a reasonable choice. This choice, and the selection of a telecentric beam expander, fixes the focal length of the first element at half the cell length.

The second beam expander element is fixed by the magnification M_{BX}. The deformable mirror was designed with a 1:1 aspect ratio with a 6 cm clear aperture. The gain region width was 1.5 cm, thus $M_{BX} = D_{DM}/W_g \cos\theta_i$, where $D_{DM} = 6$ cm, W_g =1.5 cm and the incidence angle θ_i is 45°. This gives M_{BX} of 2.82. For a telecentric beam expander, $f_2 = M_{BX} f_1$, thus $f_2 = 106$ cm.

The deformable mirror is placed at the image plane of the center of the cell.

Since the beam expander and feedback mirror are both cylindrical, the magnification M_x can be chosen independently from M_y. For such a resonator, the feedback fraction $1 - \delta$ is:

$$1 - \delta = \frac{1}{M_x M_y} \tag{4}$$

with $M_y > M_x$. The output fraction is reduced slightly by practical considerations since we elected to use an oversize cylindrical secondary. This is necessary if the Magnification is to be adjusted in this direction. Since we expect to use low magnifications in the s direction ($M_x \approx 1.07$) this is a relatively small effect. Furthermore, it does not affect the light that is fed back, and thus will have a minimal effect on performance.

4. ADAPTIVE OPTICS SYSTEM

The optical path of the index compensation control system is included in Figure 4. The adaptive optics element in the unstable resonator is a flat plate metal mirror that is controlled to deform to the conjugate of the wavefront error introduced by the index gradient. The mirror is driven to the required shape by two very stiff, long-stroke magnetostrictive actuators developed especially for this application. A double pair of Hartmann-Shack wavefront tilt sensors monitor the error being introduced as the pumping occurs and provide a signal to a closed loop digital control system. The mirror can also be driven to a desired shape independently of the wavefront sensors using position sensors that measure the tip, tilt and cylinder of the mirror. A full description of the deformable mirror and its control system is given in a companion paper. [13].

4.1 Deformable mirror

A plate element subjected to pure bending moments at the boundary deforms to a cylinder, which for the small included angle of arc is virtually the desired parabola. Introducing a uniform bending moment with only two actuators is accomplished by sculpting the edges of the plate to distribute the actuator forces equally. Further improvement in bending fidelity across the clear aperture is achieved by oversizing the mirror to reduce the edge effects. The mirror was fabricated from a bare polished

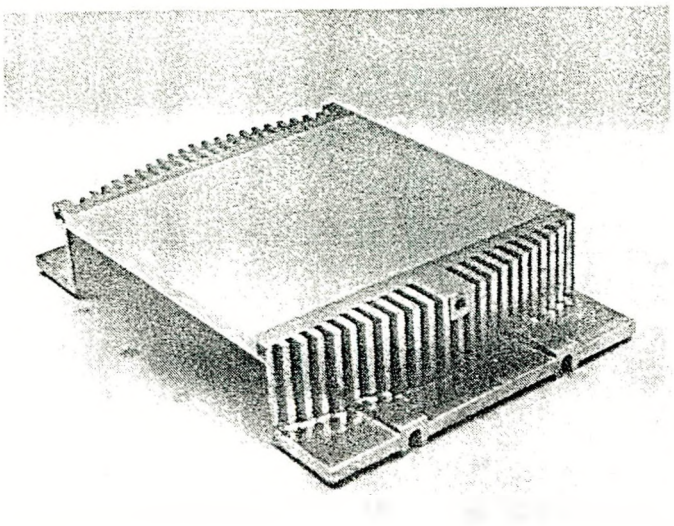

Figure 5: The sculpted edges of the titanium substrate distribute the actuator forces along the boundary of the deformable mirror producing a nearly uniform bending moment.

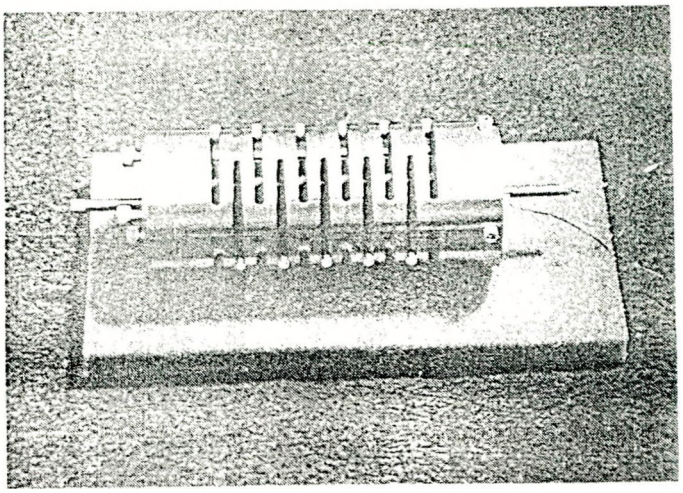

Figure 6: A magnetostrictive actuator with the preload spring (actuator casing). Within the casing are the permanent magnets (SmCo), a coil and the nested Terfenol-D^{TM} rods. The end pole pieces incorporate integral flexural elements for mounting.

titanium substrate and coated with sputtered gold. Figure 5 shows the finished deformable mirror substrate.

4.2 Magnetostrictive Actuator

The desired amplitude vs time bending profile of the mirror must produce a convex cylinder across a 6 cm clear aperture with approximately 12 μm sag in a 10 msec pulse. This profile includes Fourier spectral components greater than 300 Hz so a very stiff actuation system is required. Actuator technologies that were considered for this application included solenoid (rejected for low efficiency and lack of stiffness), microstepping motor (rejected due to high quiescent currents, potential backlash difficulties and marginal slew rate capability), lead zirconium titanate (PZT) and lead manganese niobate (PMN) electrostrictive stacks (rejected because of length of stack to achieve stroke and very high pulse current requirements) and a magnetostrictive material (Edge Technologies Etrema Terfenol-D^{TM}).

Magnetostriction is a characteristic of some metals, particularly iron when alloyed with the rare-earth elements terbium and dysprosium. The strain produced when this material is subjected to a magnetic field is on the order of 1000 to 2000 ppm depending on the process used in manufacturing the material and the magnetic coupling efficiency of the actuator design. The material is particularly suitable for pulse stroke applications. "Stroke and hold" applications are less favorable because of the dc current requirements and the resultant power dissipation.

The actuators designed for this application (see Fig. 6 and 7) include a single rod design with 75 μm stroke and a nested two rod design with 130 μm stroke. Both designs include permanent magnets to bias them at the midpoint (single rod) and near the maximum stroke (nested rod) in order to achieve the proper stroke direction when driven by a coil current that produces additive or subtractive magnetic fields during operation. Two single rod actuators are used to dynamically remove tip and tilt in the mirror while two nested rod actuators introduce the cylinder. Both designs incorporate a preload spring (which optimizes the magnetostrictive efficiency) and have fundamental resonances above 500 Hz. The actuators are attached to the mirror substrate and the support structure with a system of flexures (see Fig. 8).

4.3 Control System

The actuators are driven by a closed loop control system using two different sensors, depending on the control mode (see Figure 9). Command mode is used to position the mirror to an arbitrary figure. This mode is helpful for set-up and for replaying recorded profiles to calibrate the system. In command mode, mirror surface displacement measurements are made in a differential manner to determine the tip, tilt and curvature of the mirror. Non-contacting Kaman KD5100 eddy current gauges are used as the sensors and calibrated to provide linear response against the titanium target. These same sensors are used as open loop sensors in active mode to record the mirror response for post-test analysis.

Active mode is the normal operational mode and uses

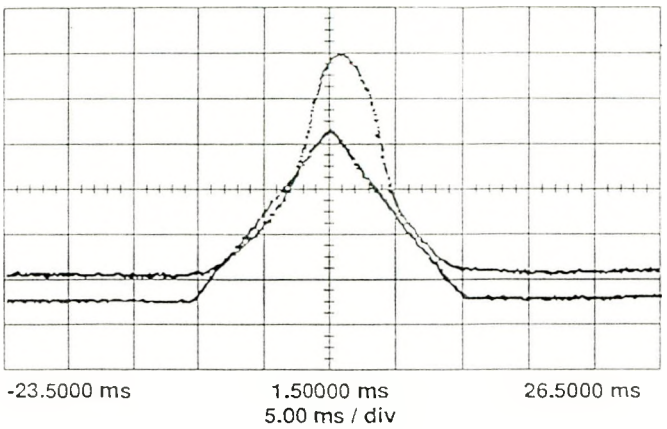

Figure 7: Response of nested rod magnetostrictive actuator to a triangular input waveform. The vertical scale of the response curve is 24 μm/division, thus 115 μ total stroke is shown.

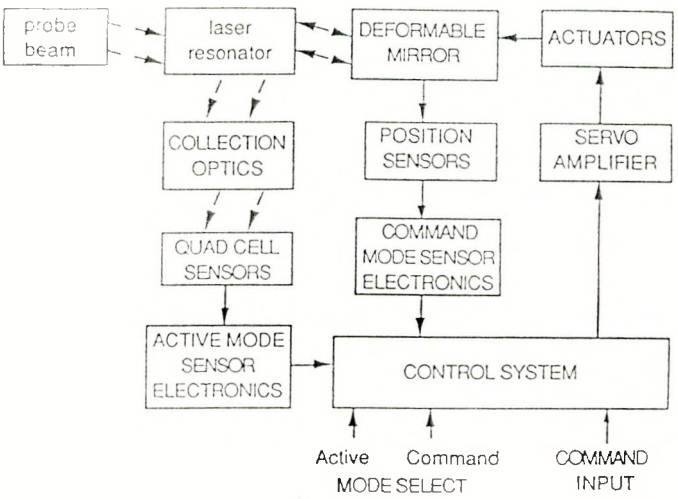

Figure 9: The shape of the magnetostrictive actuator driven deformable mirror is controlled by either a position sensed command control loop or a wavefront sensed active control loop.

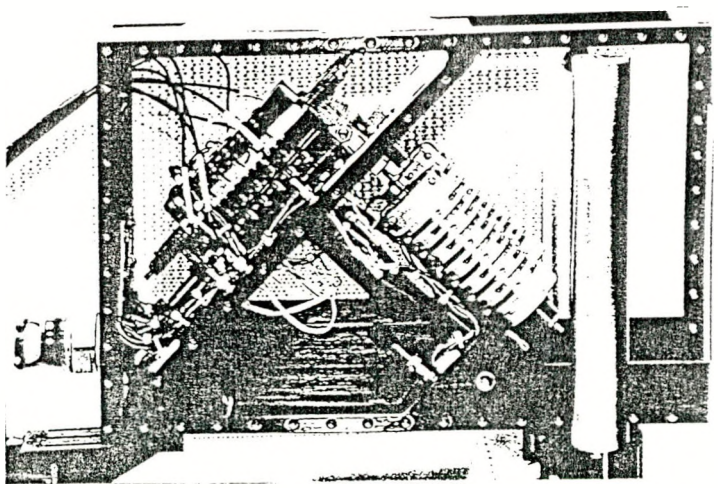

Figure 8: The completed deformable mirror assembly showing two tip/tilt actuators, the titanium mirror substrate and two cylinder actuators. The mirror surface displacement gauges are also shown.

a probe beam directed through the lasing gas to sample the index changes. The beam encounters the deformable mirror and is reflected to the optical sensors. Optical tilt information from each of its four corners is obtained using Hartmann-Shack wavefront sensors. The four tilt sensor signals are input to analog to digital converters and filtered, combined and weighted to produce full aperture mirror tip, tilt and curvature error signals.

The signals from the displacement gauges (in command mode) or the tilt sensors (in active mode) are processed to produce a second order closed loop control system to minimize the surface error. The control system is implemented on a Motorola 56000 Digital Signal Processor (DSP) installed in an AT-compatible host interface personal computer.

5. RESONATOR MODELLING

The resonator is designed using geometric optics concepts and paraxial ray tracing with 2×2 ray matrixes. A ray-tracing computer code is used for detailed analysis to check alignment and design sensitivities. Once the ray tracing has been used to design the resonator, physical optics modelling can be used to predict the laser output intensity and phase.

5.1 Geometric Optics Modelling

The first step in the design and modelling of a resonator is to understand its geometric performance. This

can be accomplished through ray-tracing and geometrical optical analysis. There are many powerful ray-tracing computer programs avaiable for this purpose, such as BEAM4[14]. The resonator is modelled by tracing rays throughout a round trip. The spacing and curvatures of the various optical elements can be adjusted by specifying targets for the round-trip rays and using the automatic optimization functions provided by these computer codes. The design task becomes one of setting up the appropriate ray goals and allowing the code to perform the appropriate optimization.

Since the gain region index field plays a large part in the overall resonator design, an appropriate model of this aberration must be included in the ray-tracing. This is complicated since most ray tracing codes are designed to handle only surfaces, not continuous media. Thus an equivalent multiple lens model of the laser gain region must be constructed.

Equations 1 through 3 present a paraxial model of the index field. The 2×2 ray matrix model of an optical element contains information about the optical element length, power and magnification. Thus an optical system made up of several surfaces can be used to model any ray matrix, if enough surfaces are included. A series of thin lenses with constant spacing is appropriate for modelling the quadratic duct. Since the quadratic duct is described by three independent parameters, we have chosen to model it with three equally spaced thin lenses. The focal lengths of the lenses are found such that the ray matrix elements of the quadratic duct and the three lens system are equal. Thus

$$\begin{bmatrix} A & B \\ C & D \end{bmatrix} = \left(\begin{bmatrix} 1 & L/2m \\ 0 & 1 \end{bmatrix} \begin{bmatrix} 1 & 0 \\ -1/f & 1 \end{bmatrix} \begin{bmatrix} 1 & L/2m \\ 0 & 1 \end{bmatrix} \right)^m \quad (5)$$

where m is the number of simple lenses used to model the ray matrix. This equation is solved for the focal length f given a length L and number of lenses m. We used an iterative method to solve equation 5 for f given L =75 cm (the laser gain region length) and $m = 3$ for different index gradient strengths γ^*. We found that an accurate solution to equation 5 is obtainable as long as $m \geq 3$. The results are plotted in Fig. 10. This allows us to model accurately the effect of distributed media using a surface oriented ray-tracing code.

The first step in the ray-tracing analysis was to optimize the beam expander element spacing for collimated output at given magnification. Once the beam expander was fixed, the appropriate equivalent lenses were used to simulate the effect of the laser medium aberrations. The deformable mirror curvature was adjusted to give a collimated output beam. The initial magnification needed to produce a collimated output beam with a flat deformable

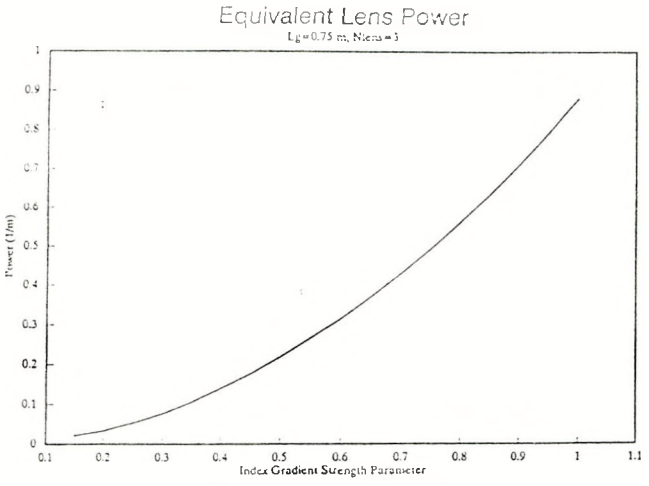

Figure 10: Equivalent lens focal length for three lenses, equally spaced in a 75 cm laser medium as a function of index gradient strength γ^*.

mirror was M_x =1.078. This magnification is consistent with results from a 2×2 ray matrix analysis model. It was necessary to adjust several of the optical path lengths in order to achieve consistent results.

By adjusting the beam expander spacing it is possible to bias the deformable mirror operating point optically, although this will affect the magnification. While it is desirable that the deformable mirror is flat during the alignment and set up stages, the design of the magnetostrictive actuators may make this difficult. The mirror is designed to allow for short periods of static curvature to allow for this possibility. The combination of initial beam expander separation, secondary mirror placement, and initial deformable mirror curvature can be used to maintain the stability of the resonator during the pumping pulse. A computer program is currently in preparation that will be used for this design process.

The key requirement for the deformable mirror are obtained from previous measurements of the wavefront time evolution[2] as presented in figure 3. Figure 11 presents some selected profiles of the wavefront at different times. These measurements are taken at conditions exactly similar to those expected for the reactor-driven experiments. This case was chosen for both high efficiency and good laser kinetics at appropriate energy and power loading[9].

The deformable mirror control system uses a Hartmann-Shack wavefront sensor to make wavefront slope measurements at four different points across the gain region aperture. Since the y-direction has been found to be relatively unperturbed by the pumping mechanism, the signal processing includes averaging the slope measurements in this direction. The wavefront slopes were calculated at ±0.53

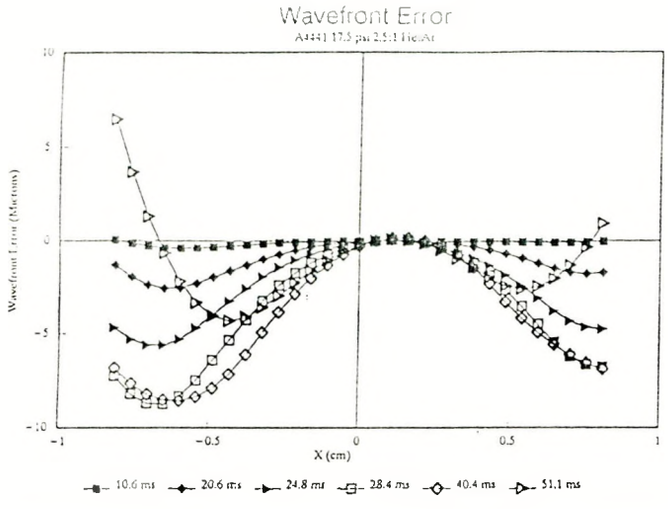

Figure 11: Measured wavefront error profiles at different times during the pumping pulse for a 60 cm laser cell.

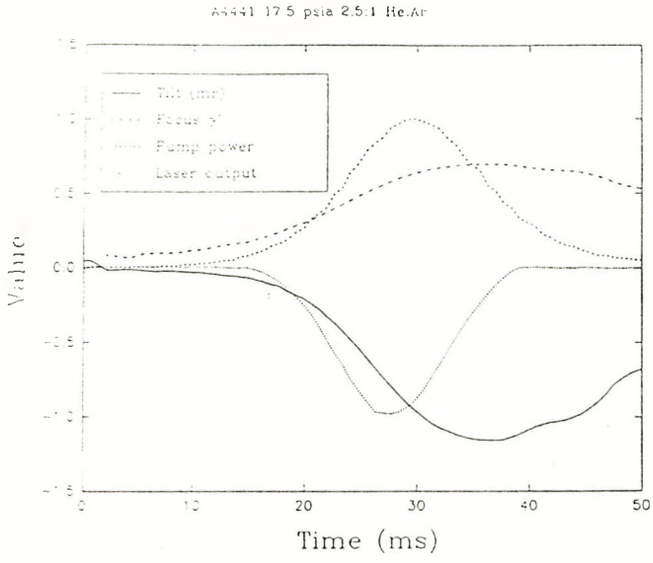

Figure 12: Time history of the measured tilt and focus (γ^*) for a 17.5 psi, 2.5:1 He:Ar gas mix. The pumping power and a stable cavity lasing pulse are also shown.

cm to simulate the finite sampling of the Hartmann-Shack wavefront sensor.

Figure 12 presents a calculation of the wavefront effective tilt and focus (expressed as γ^*) from the wavefront measurements. The reactor power and stable cavity laser output power are also shown on Fig. 12 in addition to the wavefront tilt and focus terms. The tilt and focus are the two inputs to the deformable mirror (except for tip, which is not expected to have a significant value). The mirror control system is designed to track the profiles shown in Fig. 12.

To predict the performance of the deformable mirror/resonator systems we computed the deformable mirror profile (assuming small tracking error) based on the tilt and focus calculations of Fig. 12. This deformable mirror profile is shown in Fig. 13 along with the original wavefront error. The difference, also shown in Fig. 13, represents the residual error after correction by the deformable mirror. Note that the residual error is large near the walls, or where the wavefront profile deviates from parabolic, but is below 0.25μm for most of the aperture.

5.2 Physical Optics modelling

Physical Optics modelling was performed with the VSOURCE program, part of the PARAXIA[15] package. This code uses the virtual source theory of Southwell[16] to solve for the resonator eigenvalues and eigenwaves. This code is very efficient, and can solve hundreds of cases in a few minutes. The only input to this code are the resonator magnification and the equivalent Fresnel number.

The equivalent Fresnel number in the x-direction was 39.9 and in the y-direction 9.04, with $M_y = 2.26$ and

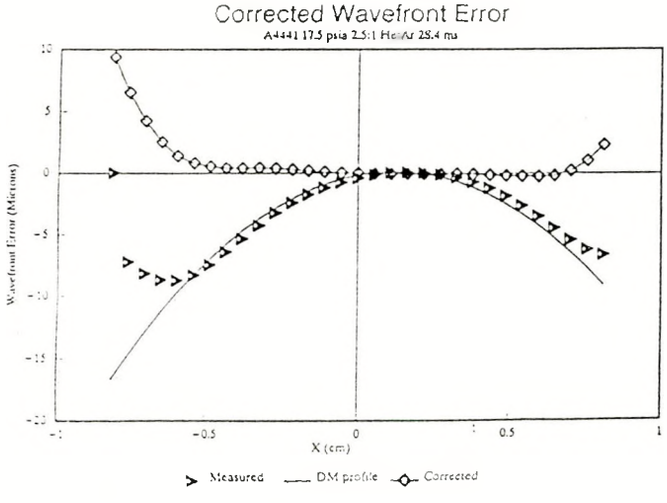

Figure 13: Measured wavefront error profile and deformable mirror surface profile. The difference (also shown) represents the residual wavefront error of the system. This data is for 17 psi, 2.1:1, He:Ar gas mixture.

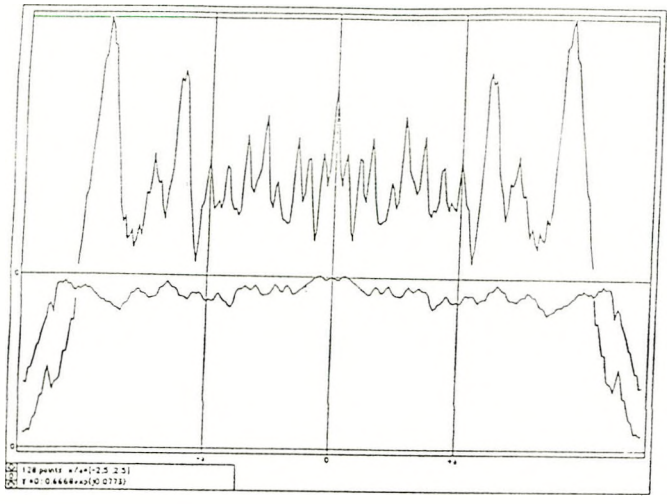

Figure 14: Eigenwave intensity and phase for the unperturbed direction for an unstable resonator with magnification $M_x = 2.26$ and Fresnel number N_{eq} =9.04.

$M_x = 1.078$ The eigenwave calculations are presented for the unperturbed y-direction in Fig. 14, and are reasonable for an unstable resonator of this type. However, preliminary results did not yield consistent eigenwaves in the x-direction. This may have been due to undersampling in this direction. More analysis is needed to resolve these ambiquities.

6. CONCLUSIONS

We have developed an astigmatic unstable resonator for use in a side-pumped laser with strong time-dependent medium index-of-refraction variations. The resonator includes an internal deformable mirror that is imaged into the gain region in order to compensate for the expected index variations. Optical path difference analysis indicates that extremely good correction should be obtainable over most of the laser aperture. However, diffractive optics calculations have yet to yield consistent results, and more modelling is necessary. Much of the hardware has been assembled and tested, and the deformable mirror has been tested through open loop operation.

7. ACKNOWLEDGMENTS

This work was performed at Sandia National Laboratories, supported by the U. S. DOE under contract number DE-AC04-76DP00789.

8. REFERENCES

1. D. R. Neal, J. R. Torczynski, and W. C. Sweatt, "Time-resolved wavefront measurements and analyses for a pulsed, nuclear-reactor-pumped laser gain region," *Optical Engineering* 29(11), 1404-1412 (November 1990).

2. D. R. Neal, J. R. Torczynski, W. J. Alford, R. B. Michie, and D. E. Bodette, "Time-dependent wavefront error measurements for a long-pulse wall-pumped laser," Conference on Lasers and Electro-Optics, May 1991.

3. D. R. Neal, W. C. Sweatt, and J. R. Torczynski, "Resonator design with an intracavity time-varying index gradient," *Current Developments in Optical Engineering*, SPIE Vol. 965, pp. 130-141, (1988).

4. U. Balucani and V. Tognetti, "Thermal effects in flashlamp-pumped dye solutions," *Optica Acta* 23 (11), 923–932 (1976).

5. P. R. Longaker and M. M. Litvak, "Perturbation of Refractive Index of Absorbing Media by a Pulsed Laser Beam," *J. Appl. Phys.* 40 (10), 4033–4041 (1969).

6. A. Corvo, "Density behavior and wavefront error for a nuclear-reactor pumped gas laser," JOSA-B, August 1991.

7. A. E. Siegman, *Lasers*, (University Science Books, Mill Valley, CA, 1986), Chap. 16.

8. J. R. Torczynski, "On the motion of a gas experiencing range-dependent volumetric heating," *J. Fluid Mech.*, submitted (1988).

9. W. J. Alford and G. N. Hays, "Measured Laser Parameters for Reactor-Pumped He/Ar/Xe and Ar/Xe Lasers," *J. Appl. Phys.*, submitted (1988).

10. R. H. Freeman and J. E. Pearson, "Deformable mirrors for all seasons and reasons," *Appl. Optics* 21 (4), 580–588 (1982).

11. A. Fuschetto, "Three-actuator deformable water-cooled mirror," *Optical Engineering* 20 (2), 310–315 (1981).

12. R. H. Sawicki and W. C. Sweatt, "Apparatus for and method of correcting for astigmatism in a light beam reflected off of a light reflecting surface," *U.S. Patent number 4,647,164*, March 3, 1987.

13. C. S. Sheppard, S. A. Cardero, D. B. McClain and K. P. Pflibsen, "Deformable mirror for pulsed mode astigmatic correction using magnetostrictive actuators," Conference on Active and Adaptive Optical Component, SPIE Proceedings Vol. 1543, July, 1991.

14. BEAM 4, Stellar Software, Berkeley, CA.

15. PARAXIA, Stanford University, Stanford, CA 94305.

16. W. H. Southwell, "Unstable-resonator-mode derivation using virtual-source theory," *J. Opt. Soc. Am.* *A*3, 1885–1891 (November 1986).